# 氧化铝基复合陶瓷 –金属钎焊界面的热应力

曲仕尧[1], 邹增大[1], 王新洪[1], 何立琴[2]
(1.山东大学 材料科学与工程学院, 济南 250061; 2.山东大学 控制科学与工程学院, 济南 250061)

摘 要: 用 Ag–Cu–Ti钎料钎焊 $SiC_w/Al_2O_3$复合陶瓷和金属时, 陶瓷与钎料发生化学反应, 在陶瓷表面形成由 TiO、TiC等物相组成的反应层。采用有限元法, 对 $SiC_w/Al_2O_3$复合陶瓷/反应层界面的热应力进行了计算。结果表明, 复合陶瓷/反应层界面的残余应力变化急剧, 最大拉应力位于晶须、基体和反应层交界处; 晶须内部及其表面存在较高的双向压应力, $Al_2O_3$基体主要承受垂直于界面的拉应力; SiC晶须/反应层界面及其附近的反应产物 TiC内具有较高的平行于界面的拉应力, 当连接界面承受剪力作用时, SiC晶须/反应层界面和 TiC处极易破坏。借助 TEM和 SEM观察了复合陶瓷/反应层界面区的精细结构和剪切断口形貌, 并利用计算结果对观察到的现象进行了分析。

关键词: 复合陶瓷 –金属钎焊; 界面; 残余应力; 有限元法
中图分类号: TG 404 文献标识码: A 文章编号: 0253–360X(2005)04–16–05

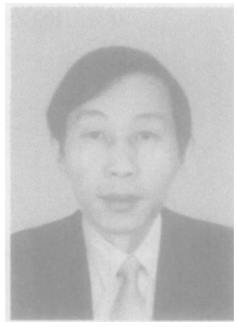

曲仕尧

## 0 序 言

陶瓷基复合材料(CMC)是一种新兴的工程结构材料, 具有耐高温、抗氧化、耐腐蚀、高硬度等一系列优异性能, 在航空、航天、军工及核能等尖端领域具有广阔的应用前景。但 CMC脆性大、韧性低、加工性能差、难以制成大型或形状复杂的构件, 因而在工程上的实际应用受到了很大限制。解决 CMC实用化的最好方法之一是将 CMC与金属连接起来制成复合构件使用[1]。

$Al_2O_3$、$ZrO_2$、$Si_3N_4$、SiC等单相陶瓷与金属的连接技术已有了较大发展, 而其中的钎焊技术发展尤为迅速。采用钎焊法连接陶瓷与金属时, 由于陶瓷和金属的线膨胀系数相差较大, 所以高温钎焊后冷却到室温时, 陶瓷 –金属接头内将产生较大的残余应力, 导致接头承载能力下降, 严重时还会出现陶瓷自裂现象。国内外学者采取多种手段对陶瓷 –金属接头的热应力进行测试和计算[2~4], 试图弄清接头内热应力的大小、分布以及影响因素, 以便找到改善接头应力状态、提高接头力学性能的有效方法。

钎焊技术在 CMC与金属的连接领域也有广阔的发展应用前景[5,6]。但 CMC是由多种不同物质组合而成的复相陶瓷, 其组织和性能与单相陶瓷差别很大, 连接起来更加困难。CMC增强相的存在不仅会改变 CMC与钎料界面的组织结构, 而且会导致界面的应力状态发生变化, 从而对界面或接头的性能产生重要影响。这种影响仅从宏观角度考察一般很难发现, 必须从微观上进行仔细研究。SiC晶须增韧 $Al_2O_3$陶瓷($SiC_w/Al_2O_3$)是由氧化物和非氧化物制成的典型复合材料, 在刀具、热机、热交换器等领域已商品化。文中采用 Ag–Cu–Ti钎料, 在氩气保护条件下对 $SiC_w/Al_2O_3$与金属实施连接, 利用有限元法(FEM), 对 $SiC_w/Al_2O_3$–钎料界面的残余热应力进行了计算, 并结合试验进行了分析讨论。

## 1 分析方法与计算模型

### 1.1 分析方法

$SiC_w/Al_2O_3$复合陶瓷 –金属钎焊接头的热应力状态十分复杂。一方面, 复合陶瓷作为一个整体, 与被连接金属间存在较大的线膨胀系数差; 另一方面, 复合陶瓷各组成相之间、组成相与连接材料或反应层之间也存在一定的线膨胀系数差。这些差异都会在钎焊接头内引起热应力。进行应力分析时, 除了复合陶瓷与金属热失配造成的应力外, 还应考虑 $SiC_w$第二相对 $Al_2O_3$基体和连接界面热应力的影响。对于如此复杂的问题, 用简单的分析方法是难以解决的, 而有限元法是解决这类问题的有效方法。文中采用功能强大的 ANSYS有限元分析软件, 对 $SiC_w/Al_2O_3$复合陶瓷 –金属钎焊接头的热应力进行分析。

收稿日期: 2004–05–08
基金项目: 山东省自然科学基金资助项目(Z2000F02)

$SiC_w/Al_2O_3$ 复合陶瓷第二相 $SiC_w$ 的尺寸通常都在微米数量级,与陶瓷制品或陶瓷 –金属接头的尺寸相差甚远。应力分析时,如果在整个接头范围内考察晶须的影响,必然会给分析计算带来很大的困难。为便于分析和突出重点,将复合陶瓷 –金属接头的热应力分为两类,即宏观应力和微观应力。宏观应力是指整个接头在温度变化时所产生的热应力,计算时把复合陶瓷视为均质材料,不考虑晶须和反应层的影响。微观应力主要指接头局部区域材料线膨胀系数不匹配引起的应力,此时不考虑整体热失配应力场的影响。$SiC_w/Al_2O_3$ 复合陶瓷/反应层界面及其邻近区域由于 SiC晶须的存在和反应产物的不同,其应力状态最为复杂,对接头的力学性能影响较大,因此文中重点对该区域的微观应力进行分析。

### 1.2 计算模型

采用 Ag–Cu–Ti活性钎料连接 $SiC_w/Al_2O_3$ 与金属时,钎料中的活性元素 Ti在高温下不断向陶瓷表面扩散并与陶瓷发生化学反应,从而在陶瓷与钎料界面形成了反应产物极为复杂的过渡层[7]。经 X射线衍射(XRD)检测和电子衍射分析,反应产物主要为 TiO、TiC、AlTi、$Ti_2O$、$Cu_2Ti_4O$ 等。其中,紧靠陶瓷表面的薄层由 TiO和 TiC组成。TiO与陶瓷基体 $Al_2O_3$ 接触,而 TiC位于增强相 $SiC_w$ 附近。

钎焊过程中,陶瓷/钎料界面反应层不仅形成于加热过程,而且在冷却过程中也可能形成。假定反应层是在连接温度(900 ℃)下形成的,即认为在升温和冷却过程中不形成反应层。实际上反应层主要是在连接温度下保温一定时间形成的,所以上述假设不会带来很大的误差。这样计算时不必考虑加热过程,而只需考虑反应层形成后从钎焊温度到室温的冷却过程。

全面考察反应层所有组成相的影响目前还存在一定困难,因为有些物相的性能参数无法获得。另一方面,与陶瓷接触的反应层对钎焊界面或接头的性能影响最大。因此,计算模型仅涉及由 TiO和 TiC组成的反应层。

钎焊接头中,复合陶瓷/反应层界面附近的晶须有些与反应层接触,有些不接触;有的与反应层垂直,有的则与反应层平行或斜交。考虑到实际钎焊接头的剪切断口上经常出现含 Si量较高的圆形区域,预计与垂直接触的晶须有关,所以以晶须与反应层垂直接触的情况为考察重点,并取单根晶须进行分析,同时忽略邻近晶须引起的应力场干扰。

计算采用的几何模型和网格划分如图 1所示。在复合陶瓷/金属钎料界面附近取包含单根晶须和反应层的微小区域,考虑到晶须的实际含量、尺寸及反应层的实际厚度[7,8],将其尺寸定为 13 μm×5 μm。其中,反应层厚度取 2 μm,晶须直径和长度分别取 1 μm 和 8 μm;与基体 $Al_2O_3$ 接触的反应产物为 TiO,与 SiC晶须接触的反应产物为 TiC。有限元分析采用 240个 8节点矩形单元,相界面附近应力变化较大,所以网格划分比较密。陶瓷和反应层均为脆性材料,冷却过程中塑性变形量很小,可忽略不计。故研究涉及的热应力问题按弹性平面问题处理,计算采用的材料性能参数见表 1。

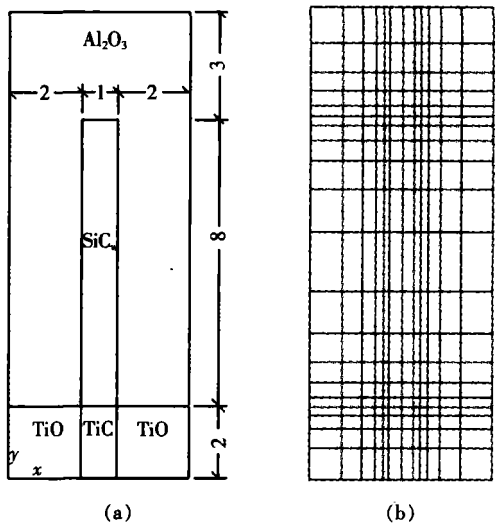


图 1　界面应力计算几何模型及有限元网格示意图(单位:μm)

Fig. 1　Illustration of geometry model and FEM mesh for stress calculation

表 1　计算热应力用的材料性能参数

Table 1　Material properties used for calculation

| 材料 | 弹性模量 $E$/GPa | 泊松比 $\mu$ | 线膨胀系数 $\alpha$/($10^{-6}$℃$^{-1}$) |
|---|---|---|---|
| $Al_2O_3$ | 402 | 0.23 | 8 |
| $SiC_w$ | 700 | 0.23 | 4.2 |
| TiO | 380 | 0.25 | 7.5 |
| TiC | 490 | 0.25 | 8.2 |

## 2　计算结果

从钎焊温度冷却到室温时,复合陶瓷/反应层界面附近残余应力的分布如图 2所示,其中图 2a为垂直于陶瓷/反应层界面的应力($\sigma_y$)分布,图 2b为平行于陶瓷/反应层界面的应力($\sigma_x$)分布。由图可见,SiC晶须两端的应力分布极其复杂,晶须 $Al_2O_3$ 基体和晶须/反应层界面存在急剧的应力变化。晶须内部受压,陶瓷基体主要受拉,而反应层的应力则比较复杂。$x$、$y$ 方向的最大拉应力分别位于晶须、

基体和反应层三者交界处或紧靠交界的晶须表面(图中标有 MX处), $\sigma_x$ 和 $\sigma_y$ 的最大值分别为 596 MPa和 433MPa

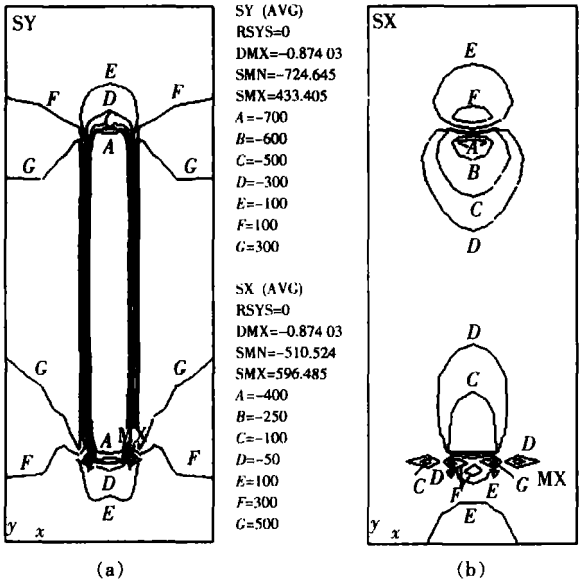


图 2 陶瓷/反应层界面区残余应力 $\sigma_y$ 和 $\sigma_x$ 的分布(单位: MPa)

Fig. 2 Distrbution of residual stresses near ceramic/reaction-layer interface

复合陶瓷/反应层界面处的残余应力沿 $x$方向的分布见图 3。SiC晶须、$Al_2O_3$ 基体和反应层交界处出现了应力集中现象,晶须端部承受较高的 $x$方向拉应力和 $y$方向压应力(约 600MPa)。晶须、基体和反应层交界承受较高的双向拉应力,且 $x$方向最高拉应力大于 $y$方向。晶须端部外侧附近的残余

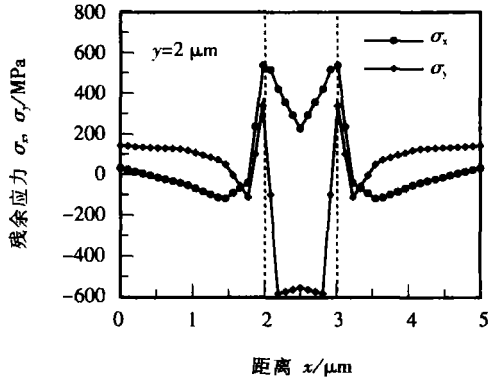


图 3 陶瓷/反应层界面残余应力沿 $x$方向的分布

Fig. 3 $x$ distribution of residual stresses at ceramic/reaction-layer interface

应力由拉应力很快转变为较低的压应力,而远离交界的界面上出现 $y$方向的拉应力。

复合陶瓷内距陶瓷/反应层界面 0.15μm处的残余应力沿 $x$方向的分布见图 4。与陶瓷/反应层界面相比,应力状态有了较大变化。该处 SiC晶须承受两个方向的压应力,并且 $y$方向的压应力幅值有所增加,晶须中心压应力最高(约 800MPa);邻近晶须的 $Al_2O_3$ 基体承受双向拉应力,但主要应力为 $\sigma_y$,而 $\sigma_x$ 的幅值非常小。

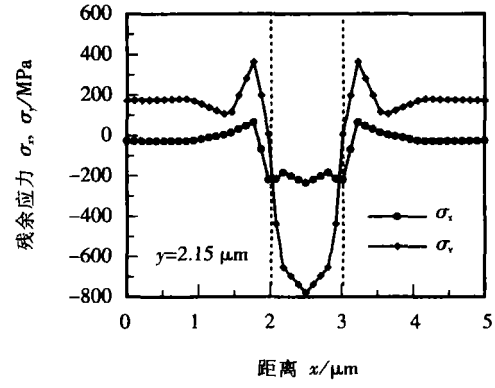


图 4 界面附近陶瓷内残余应力沿 $x$方向分布

Fig. 4 $x$ distrbution of residual stresses in ceramic near ceramic/reaction-layer interface

在反应层中,距陶瓷/反应层界面 0.2μm处的残余应力沿 $x$方向的分布如图 5所示。TiC承受较高的 $x$方向拉应力和大小在 200~300MPa范围内波动的 $y$方向压应力;TiC/TiO界面及其附近的 TiO承受双向压应力,远离该界面的 TiO承受 $y$方向拉应力,而 $x$方向的应力基本为 0。

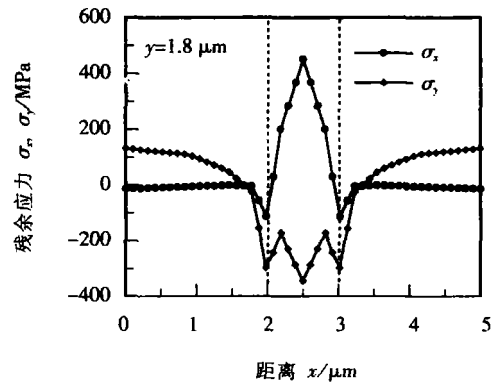


图 5 界面附近反应层内残余应力沿 $x$方向分布

Fig. 5 $x$ distribution of residual stresses in reactive layer near ceramic/reaction-layer interface

图 6是 $x=2$μm、与晶须侧表面和 TiC/TiO 界面对应处的残余应力沿 $y$方向的分布情况。由图可见,晶须和反应层交界处承受较大的双向拉应力;在 TiC/TiO界面上,靠近晶须处承受双向压应力,远离晶须处承受 $x$方向拉应力,且距晶须越远,拉应力越

大;晶须侧表面主要承受 $y$方向压应力,中部压应力最大,端部则较小并逐渐转变为拉应力;晶须上端部的陶瓷基体承受 $x$方向拉应力和 $y$方向压应力,远离晶须端部处应力为 0。

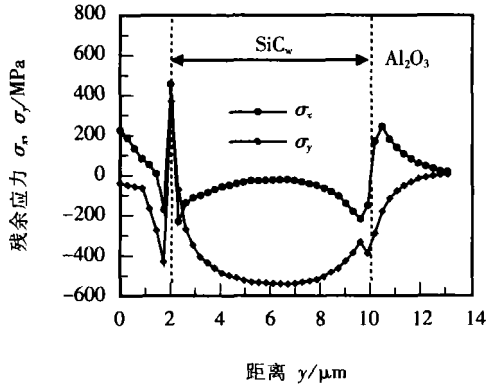


图 6　残余应力($x$= 2μm)沿$y$方向的分布

Fig. 6　$y$ distrbution of residual stresses at $x$= 2μm

## 3　分析与讨论

复合陶瓷 /反应层界面附近微观应力的有限元分析结果表明,该界面附近残余应力的分布极不均匀,在 $Al_2O_3$ 基体 /SiC 晶须界面、陶瓷 /反应层界面等部位均出现了峰值较高、变化急剧的残余应力。最高拉应力出现在晶须、基体、反应层三者交界处(图 2);晶须内部及表面出现了以 $y$ 方向正应力 $\sigma_y$ 为主的双向压应力 (图 4,图 6),陶瓷基体主要受拉,且以 $y$方向拉应力为主(图 4);在陶瓷 /反应层界面上,SiC 晶须端面出现了数值较高的 $y$方向压应力和 $x$方向拉应力(图 3);在晶须、陶瓷基体和反应层交界处,存在较高的双向拉应力 (图 6);在反应层中,陶瓷 /反应层界面附近的 TiC 承受较高的 $x$方向拉应力和 $y$方向压应力 (图 5),远离界面处则相反 (图 2);界面附近的 TiO 主要承受 $y$方向拉应力,而 TiO /TiC 界面承受 $x$方向拉应力(图 6)。

复合陶瓷 /反应层界面产生较高的残余应力和应力梯度的主要原因在于异种材料的线膨胀系数不同。当然,弹性模量的差异对残余应力也会产生一定影响。从表 1列出的数据可见,SiC 晶须的线膨胀系数最低,约为 $Al_2O_3$ 基体的一半。因此从钎焊温度冷至室温时,在 $Al_2O_3$ 基体中产生了较大的拉应力,而在 $SiC_w$ 中出现了较大的压应力。由于陶瓷基体延性低、脆性大、抗拉能力弱,所以当基体内拉应力达到一定数值后,便会在基体的缺陷或应力集中部位引发裂纹;拉应力继续增大时,裂纹便在基体中迅速扩展。然而,由于晶须内部及晶须 /基体界面附近存在较大的压应力,所以当裂纹扩展到晶须表面附近时,其扩展速度将会减缓,甚至其扩展受到阻碍而改变扩展方向。

文中借助透射电镜 (TEM)对 $SiC_w$ /$Al_2O_3$ 陶瓷与金属钎焊界面的精细结构进行了观察。图 7是典型的复合陶瓷 /反应层界面附近陶瓷的微观结构 TEM 图像。由图可见,裂纹在陶瓷基体中形成并在基体内扩展,一旦遇到 SiC 晶须,裂纹便发生偏转并绕过晶须继续扩展,或者在晶须表面终止扩展。实际接头的裂纹扩展行为与前面的计算和分析非常吻合。裂纹的偏转扩展通常比直线扩展需要消耗更多的能量,从而使材料的断裂韧性显著提高,此即晶须增韧机制之一。

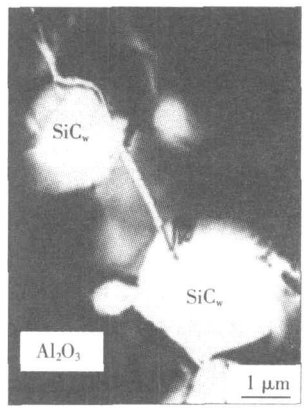


图 7　界面附近复合陶瓷微观形貌(TEM)

Fig. 7　TEM image of ceramic near interface

陶瓷 /金属连接界面常常是整个接头的薄弱环节。当陶瓷材料含有成分、性能与基体差异比较大的第二相时,必须考虑第二相对连接界面性能的影响。对于 $SiC_w$ /$Al_2O_3$ 复合陶瓷,$SiC_w$ 的存在一方面改变了界面反应层的组成和结构,另一方面在界面附近引起较高的局部热应力。从前面的计算结果来看,晶须端部、陶瓷基体和反应层交界处应力最大,是复合陶瓷 /反应层界面最危险的部位之一,有可能成为裂纹的起源和破坏的起点。另外,在 SiC 晶须 /反应层界面及 TiC 反应产物中,均出现了较高的平行于陶瓷 /反应层界面的拉应力。因此,当陶瓷 /金属接头受到平行于连接界面的剪力作用时,极易从 SiC 晶须的端面和 TiC 反应产物处破坏。

图 8是采用 Ag – Cu – Ti钎料连接的 $SiC_w$ / $Al_2O_3$ –金属钎焊接头中典型的剪切断口形貌。照片中部出现了形貌特征与其周围不同的圆形区域。经 EDX 检测,圆形区域的主要成分是 Si、Al和 Ti (见表 2)。据此可以断定,该区紧靠着 SiC 晶须。但其尺寸要比单根晶须的直径大得多,可能是多根

晶须密集于此的缘故。这种情况可按直径较粗的单根晶须处理,因此仍可利用前面的计算结果加以解释。分析认为,在钎焊接头受到平行于连接界面的剪力作用时,裂纹沿着连接界面的薄弱部位扩展;当扩展到晶须/反应层界面附近时,由于此处存在较大的平行于界面的局部应力和应力集中,与外加应力叠加后,导致晶须端面附近应力急剧增大,所以裂纹扩展转向晶须/反应层界面,因而形成了图 8所示的断口形貌。由此可见,这种断口形貌与 SiC晶须引入的局部热应力存在密切关系。

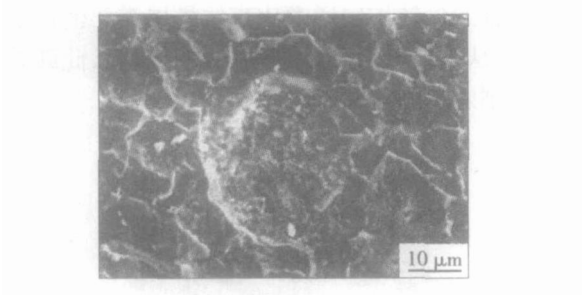


图 8 钎焊接头剪切断口形貌(SEM)

Fig. 8 SEM image of fracture surface for brazed joint

表 2 图 8剪切断口圆形区域平均成分(EDX)

Table 2 EDX results of round area on fracture surface in Fig. 8

| 元素 | Al | Si | Ti | Cu | Ag |
|---|---|---|---|---|---|
| 摩尔分数(%) | 28.92 | 34.63 | 26.12 | 6.97 | 3.36 |

## 4 结 论

(1) $SiC_w/Al_2O_3$复合陶瓷/反应层界面附近区域的热应力分布极不均匀,$Al_2O_3$基体/SiC晶须界面、陶瓷/反应层界面均出现了峰值很高、变化急剧的残余应力,最高拉应力位于晶须、基体和反应层交界处。

(2) SiC晶须内部及其表面存在较高的双向压应力,$Al_2O_3$陶瓷基体主要承受垂直于连接界面的拉应力。基体内的裂纹扩展到晶须表面时,因压应力的存在将发生偏转或终止于晶须表面。

(3) SiC晶须/反应层界面及其附近的反应产物 TiC内存在较高的平行于界面的拉应力。当连接界面承受剪力作用时,SiC晶须/反应层界面和 TiC处极易破坏。

参考文献:

[1] 任家烈, 吴爱萍. 先进材料的连接[M]. 北京: 机械工业出版社, 2000.

[2] Munz D, Sckuhr M A, Yang Y. Thermal stresses in ceramic metal joints with an interlayer[J]. J. Am. Ceram. Soc., 1995, 78(21): 285-290.

[3] Levy A. Thermal residual stresses in ceramic to metal brazed joints[J]. J. Am. Ceram. Soc., 1991, 74(9): 2141-2147.

[4] 程大勇, 陆善平, 郭 义. 陶瓷/金属钎焊接头内残余应力计算[J]. 材料研究学报, 2000, 14(1): 49-52.

[5] Dixon D G. Ceramic matrix composite metal brazed joints[J]. J. Mater Sci, 1995, 30: 1539-1544.

[6] Nakamura M, Shigematsu I. Joining of carbon fiber reinforced silicon nitride composites with 72Ag-26Cu-2Ti filler metal[J]. J. Mater Sci, 1996, 31: 4629-4634.

[7] 曲仕尧. 氧化铝基复合陶瓷-金属连接界面研究[D]. 天津: 天津大学, 2001.

[8] 邓建新. SiC晶须增韧 $Al_2O_3$陶瓷刀具材料的性能研究[D]. 济南: 山东工业大学, 1990.

作者简介: 曲仕尧, 男, 1963年 1月出生, 工学博士, 副教授. 山东大学入站博士后。主要从事焊接冶金、新材料连接研究。曾获山东省科技进步奖 2项, 发表论文 20余篇。

Email: sduqsy@sdu.edu.cn

[上接第 15页]

磨损的双层热喷涂层[J]. 中国表面工程, 2000(2): 43-48.

[10] Hu Zhijun, Ma Shining, Chen Xuerong, *et al*. Erosion-corrosion wastage at elevated temperature of arc spraying composite coatings on boiler tube of coal thermal power station[J]. Transactions of the China Welding Institution, 2003, 24(6): 12-14.
胡志军, 马世宁, 陈学荣, 等. 几种高速电弧喷涂层高温冲蚀磨损性能[J]. 焊接学报, 2003, 24(6): 12-14.

[11] Qian G, Nakamura T, Berndt C C, *et al*. Tensile toughness test and high temperature fracture analysis of thermal barrier coatings[J]. Acta Mater, 1997, 45: 1767-1784.

[12] Volinsky A A, Schneider N R, Gerberich W W. Toughness measurements for thin films on substrates[J]. Acta Materialia, 2002, 50: 441-446.

[13] Thurn G, Schneider G A, Bahr H A, *et al*. Toughness anisotropy and damage behavior of plasma sprayed $ZrO_2$ thermal barrier coatings[J]. Surface and Coatings Technology, 2000, 123: 147-158.

[14] Aditad Vasinonta, Jack L Beuth. Measurement of interfacial toughness in thermal barrier coating systems by indentation[J]. Engineering Fracture Mechanics, 2001, 68: 843-860.

[15] [illegible]谷壮 他. 最新材料力学[M]. 东京: 朝倉[illegible]店, 1990. 178-180.

作者简介: 徐连勇, 男, 1975年 10月出生, 博士研究生。主要从事焊接结构强度与断裂及热喷涂层界面断裂机理方面的研究, 发表论文 6篇。

Email: xulianyong75@163.com

# MAIN TOPICS, ABSTRACTS & KEY WORDS

**Numerical simulation of dynamic recrystallization of friction welding under electric field** LI Qing-hua, LI Fu-guo, FU Li (College of Materials Science and Engineering, Northwestern Polytechnical University, Xi'an 710072, China). p1-4

**Abstract**: The plastic deformation of welding interface material is the essence of friction welding. This paper studied the continuous driving friction welding of LY12 alloy that is often used as aerospace structure material. The plastic deformation on a rod sample of coupled thermal-mechanical analysis model under the electric field based on finite element method was established. Some physical parameter fields about the welding interface material, such as temperature field, strain field and electric field, were calculated. A Yada grain size model was used to predict dynamic recrystallization and grain size growth of the friction welding process. The welding process and the welding quality affected by these physical parameter fields was also analyzed.

**Key words**: friction welding; coupled thermal-mechanical behavior; dynamic recrystallization; electric field

**Structure characteristics and evolution at wedge bonding interface** LI Jun-hui, HAN Lei, TAN Jian-ping, ZHONG Jue (College of Mechanical-Electronical Engineering, Central South University, Changsha 410083, China). p5-8

**Abstract**: A series of experiments was carried out on structure characteristics and evolution at the bond interface. Bond lift-off characteristics were studied by using scanning electron microscope with energy dispersive spectroscope. Power characteristics of piezoelectric transducer were analyzed by the driving electric signal measured. Results show that the pattern of partially bonded material at the Ni-Al interface of ultrasonic wedge bonds exposed by peeling underdeveloped bonds simulates a ridged torus with an unbonded central and external region rubbed along pulse direction. Bonding strength is located between the severely ridged torus and the non-adhering central and external area of the bond. For the same variables, ridge peak and transforming ultrasonic energy of first wedge bonding are greater than that of second wedge bonding. For other variables constant with increasing load, the total area of bond pattern increases in size, and minor axis of torus extends major axis with increasing time; the ridged periphery spreads a whole torus, and the ridged location of the bonded region moves closer to the bond center; the sliding trace and the ridge-like of the bond pattern strengthen when more power applied.

**Key words**: electronics packaging; wedge bonding; structure; ultrasonic

**Simulation of pulse submerged arc welding dynamic process** LI Huan[1], LIU Qiong[1], YANG Li-jun[1], GUO Sheng[1], WANG Qing-guo[2], YE Chang-jun[2], TIAN Peng[2] (1. Tianjin University, Tianjin 300072, China; 2. Huayou Steel Tube Limited Liability Company, Qingxian 062650, Hebei, China). p9-12

**Abstract**: Aiming at the characteristic of pulse submerged arc welding process with change wire-feed system, the simuloting model was developed by the software of MATLAB/SIMULINK which consists of the main circuit simulation model, arc load system simulation model and arc changing system simulation model. The experimental waveform is consistent with the simulating result, which validates the correctness of the model and lies the foundation of application of pulse submerged-arc welding process.

**Key words**: change wire-feed adjusting system; pulse submerged arc welding; SIMULINK; dynamic simulation

**Measuring of Young's modulus of coatings by high velocity arc spraying** XU Lian-yong[1], JING Hong-yang[1], HUO Li-xing[1], ZHANG Yu-feng[1], MA Chong[2] (1. School of Material Science & Engineering, Tianjin University, Tianjin 30072, China; 2. Tianjin Electrical Science Research Institute, Tianjin 30072, China). p13-15, 20

**Abstract**: An effective three-point bending test based on compound beam theory is introduced. The Young's moduli of FeCrAl coatings and NiCr coatings by high velocity arc spraying are measured through three-point bending test. The results show Young's modulus of coatings are much less than that of corresponding spraying wire. The analysis indicates that the lower Young's modulus is induced by inherent characters of coatings. The flaws such as pores in the coatings result in that the actural bulk of coating is less than macroscopical bulk of coating. The reason that Young's modulus of FeCrAl coatings is less than that of NiCr coatings is that the porosity and metal particle size of FeCrAl coatings are larger than those of NiCr coatings.

**Key words**: high velocity arc spraying coatings; Young's modulus; compound beam; three-point bending; porosity

**Thermal residual stresses near interface brazing alumina matrix composite to metal** QU Shi-yao, ZOU Zeng-da, WANG Xin-hong, HE Li-qin (Shandong University, Jinan 250061, China). p16-20

**Abstract**: The chemical reaction of the composite with the brazing alloy takes place and the reaction layer composed of TiO, TiC and so on forms on the composite surface when $SiC_w/Al_2O_3$ composite is brazed to metals using Ag-Cu-Ti brazing filler alloy. The thermal residual stresses near the composite/reaction layer interface were calculated by finite element method. The results have shown that the residual stresses near

the interface change abruptly, and the highest tensile stress appears at the intersection of the whisker, matrix and reaction layer. High compressive stresses develop in the whisker and on its surface, while the $Al_2O_3$ matrix is mainly subjected to the tensile stress perpendicular to the interface. The high tensile stress parallel to the interface exists at the whisker/reaction layer interface and in TiC near the interface, at which failure occurs easily when shear force is applied. Microstructure of the interface region and shear fracture surface of the brazed joints are observed by transmission electron microscope and scanning electron microscope, and the phenomena are analyzed from the calculated results.

**Key words**: ceramic matrix composite; metal brazing; interface; residual stress; finite element method

**A network control system of welding machines based on Ethernet**

SHI Yu[1], FAN Ding[1], SONG Jian[2] (1. State Key Lab of Gansu New Non-ferrous Metal Materials, Lanzhou University of Technology, Lanzhou 730050, China; 2. College of Modern Network Education, Lanzhou University of Technology, Lanzhou 730050, China). p21-24

**Abstract**: A network control system for welding machine based on Ethernet is described. The author utilize the embedded gateway combining with micro-control unit controlling system to fulfill the welding machine connection with Ethernet, which could integrate the welding machine with company information system based on Ethernet and TCP/IP completely, and which could make possible of remote management during the welding production and remote diagnosis of welding machine faults via Ethernet. Utilizing SQL SERVER software, the Net welding machine managing system was designed, and welding standard database and welding process supervision database were constructed based on web were developed. The whole system could fulfill the maintenance of welding criterion database, the remote supervision of welding machine parameters and the remote setup of welding criterion and management based on Net work.

**Key words**: network controlled welding machine; Ethernet; embedded gateway; database

**Numerical simulation on discontinuous welding of a hot tap structure**

XUE Xiao-long[1], SANG Zhi-fu[1], JIANG Wei-zhong[2] (1. College of Mechanical and Power Engineering, Nanjing University of Technology, Nanjing 210009, China; 2. Yangzi Petrochemical Maintenance and Installation Co. Ltd., Nanjing 210048, China). p25-28

**Abstract**: The temperature field and residual stress distribution of discontinuous welding on an orthogonal nozzle were simulated and compared with the results of continuous welding. It can be concluded that the local high temperature can be reduced effectively using the technique of discontinuous welding and smaller residual stresses are obtained. The metallographic analysis shows that the metallurgical structure is proper. The results of internal pressure test indicate that the hot tap structure can work safely.

**Key words**: discontinuous welding; temperature fields; stress fields; numerical simulation; metallographic analysis

**Constitutive relations on creep for 63Sn37Pb soldered joints**

YAN Yan-fu, LIU Jian-ping, SHI Yao-wu, LI Rong (Department of Materials Science and Engineering, Beijing University of Technology, Beijing 10002, China). p29-32, 36

**Abstract**: A new high temperature creep strain equipment was used to test materials for the micro-electronic technology and soldered joints. Based the Dorn equation measurements were conducted on 63Sn37Pb joints for confirming the creep parameters, i.e., stress exponent, creep activation energy and constant. The final constitutive equation for the soldered joints was established, which demonstrated the dependence of steady-state creep rate on the stress and temperature. Results showed that the stress exponent and creep activation energy are lower than those of soldered joints, which means that the creep resistance of 63Sn37Pb soldered joints is better than that of solder. This is to say, the creep behavior of solder itself don't deducted one of soldered joints.

**Key words**: 63Sn37Pb; soldered joints; creep; constitutive relations; Dorn equation

**A model of artificial neural network for optimizing technological parameter of friction welding of dissimilar material**

WANG Yu, GAO Da-lu, LIAO Ming-fu, FENG Jing (Department of Mechanical Engineering, Northwestern Polytechnical University, Xi'an 710072, China). p33-36

**Abstract**: Aiming at to difficulty to determine the parameter correctly for dissimilar material with different thermal properties, a new method for predicting key welding parameters was introduced, which was developed on the basis of the three layers of back-propagation neural network. The result showed that the predicting values are well identical with the experimental ones.

**Key words**: friction welding; forging pressure; friction period; neural network

**Distortion research on projection welding of car door hinge—Part I: processes simulation of projection welding based on coupled finite element method**

LUO Ai-hua, CHEN Guan-long, LAI Xin-ming, ZHU Wen-feng (BMTC, Mechanical and Power Engineering School, Shanghai Jiaotong University, Shanghai 200030, China). p37-40

**Abstract**: As a part of the efforts on distortions analysis of projection welding of car door hinges, a 2D finite element model has been established based on the projection welding of car door hinges. The simulation of whole projection welding processes was performed by a coupled finite element method and the results of projection welding processes, such as the projection collapse mechanism, the nugget formation process and the distribution of temperature after weld, were discussed. Compared with the test results, good conclusions have been achieved. A well base for the